ACS APPLIED MATERIALS & INTERFACES

Research Article

www.acsami.org

Design of Au@ZnO Yolk–Shell Nanospheres with Enhanced Gas Sensing Properties

Xiaowei Li, Xin Zhou, Hang Guo, Chen Wang, Jiangyang Liu, Peng Sun,* Fengmin Liu, and Geyu Lu*

State Key Laboratory on Integrated Optoelectronics, College of Electronic Science and Engineering, Jilin University, Changchun 130012, People's Republic of China

Supporting Information

ABSTRACT: The Au@ZnO yolk–shell nanospheres with a distinctive core@void@shell configuration have been successfully synthesized by deposition of ZnO on Au@carbon nanospheres. Various techniques were employed for the characterization of the structure and morphology of as-obtained hybrid nanostructures. The results indicated that the Au@ZnO yolk–shell nanospheres have an average diameter of about 280 nm and the average thickness of the ZnO shell is ca. 40 nm. To demonstrate how such a unique structure might bring about more excellent gas sensing property, we carried out a comparison of the sensing performances of ZnO nanospheres with different inner structures. It was found that Au@ZnO yolk–shell nanospheres exhibited an obvious improvement in response to acetone compared with the pure ZnO nanospheres with hollow and solid inner structures. For instance, the response of the Au@ZnO nanospheres to 100 ppm acetone was about 37, which was about 2 (3) times higher than that of ZnO hollow (solid) nanostructures. The enhanced sensing properties were attributed to their unique microstructures (porous shell and internal voids) and the catalytic effect of the encapsulated Au nanoparticles.

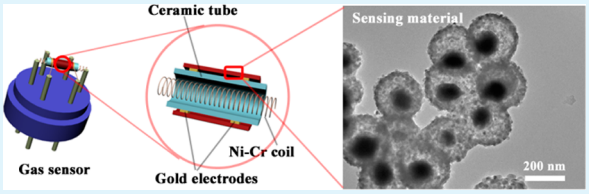

KEYWORDS: *Au@ZnO nanospheres, carbonaceous template, acetone sensor*

1. INTRODUCTION

For many years, gas sensors have received considerable attention because of their important applications in detecting toxic and deleterious gases, supervising air quality, and monitoring human health.[1−4] Owing to their excellent properties such as low cost, easy synthesis, and high sensitivity, oxide semiconductors are considered to be one of promising gas sensing materials.[5] It is well-known that the sensing mechanism can be explained by the change in resistance caused by the adsorption of oxygen and reaction with test gas molecules on the surface of oxides. Therefore, the sensing properties of semiconductor oxides is usually influenced by their chemical composition, morphologies and microstructures.[6] As motivated by the driving force of developing semiconductor oxides with enhanced sensing performance, great efforts have been exhausted on the design of novel types of materials with subtle architectures or configurations. At present, numerous distinct structures have been prepared, such as flowerlike,[7,8] bundlelike,[9] urchinlike architectures,[10] hollow microcubes,[11] hollow spheres,[12,13] core–shell nanostructures.[14−17]

Among these advanced architectures, the yolk–shell structured materials with nanoparticle cores inside hollow shells have stimulated a great deal of research interest due to their appealing structures, and controllable chemical composition. The adjustability and functionality in both cores and hollow shells endow the yolk–shell structured materials with various new properties, which will make them attractive for applications in solar cells,[18] drug/gene delivery,[19] lithium-ion batteries,[20,21] nanoreactors,[22] and catalysis.[23] For example, many previous reports have demonstrated that the yolk–shell nanospheres with noble metal cores could improve the catalytic activity in several important fields.[24−27] Encapsulating noble metal nanoparticles in a protective shell could effectively isolate metal cores and increase their stability against undesirable aggregation during practical operation.[28] Furthermore, the movable noble metal cores and the abundant active sites on the outer shell would facilitate the process of catalytic reaction.[29,30] Therefore, noble metal cores@semiconductor shell nanocomposites have been recognized as a promising functional material and a number of corresponding architectures have been synthesized in the past few years, including Au@SiO_2,[26] Au@TiO_2,[31] Ag@Fe_2O_3,[32] Pd@SiO_2,[33] Pt@CeO_2,[34] and so on. Despite much progress has been made in the design and preparation of such structured materials, the main usage of them is still limited to catalyst. Until now, only a few noble metal cores@semiconductor shell nanocomposites have been applied in gas sensors. Considering the catalytic effect of noble metal cores,[35−37] and the hollow space between the core and shell, which will benefit the diffusion of the test gases, it is reasonable to expect that such novel composites can be a good candidate for gas sensing materials.

In this paper, we present a facile and green method for the synthesis of Au@ZnO yolk–shell composites by using Au@

Received: June 20, 2014
Accepted: October 7, 2014
Published: October 7, 2014

carbon nanospheres as template. It is worth mentioning that the ZnO shell can be easily decorated on the Au@carbon nanospheres by a facile aging process at room temperature (25 °C). Moreover, a comparative sensing investigation between the gas sensors based on ZnO nanospheres with different inner structures was performed. The results indicated that Au@ZnO yolk−shell nanospheres exhibited an ultralow detection limit (200 ppb) and a dramatic enhancement in response to acetone compared with the pure ZnO nanospheres with hollow and solid inner structures. The observed improvement in sensing performance was ascribed to the catalytic effect of Au particles and the unique structure of Au@ZnO yolk−shell nanospheres.

2. EXPERIMENTAL PROCEDURE

2.1. Synthesis of Au@ZnO Yolk−Shell Nanospheres. All the reagents in the experiment were purchased from Sinopharm Chemical Reagent Co.,Ltd. and directly used as received without further purification. In a typical process, 0.4 mL of $HAuCl_4$ solution (0.05 M) was dropwise added into 30 mL of as-prepared 0.6 M aqueous glucose solution. After vigorous stirring for 30 min at room temperature, the mixture solution was transferred into a Teflon-lined stainless steel autoclave and reacted at 180 °C for 6 h. The resulting precipitate was washed with deionized water and absolute ethanol by centrifugation several times, and dried at 80 °C. After that, the brown power was annealed at 450 °C for 2 h under inert atmosphere and the Au@carbon nanospheres were finally obtained. For the synthesis of Au@ZnO yolk−shell nanostructures, 50 mg of as-synthesized Au@carbon nanospheres were dispersed by ultrasonication in 20 mL of 1.0 M aqueous zinc acetate solution. The resulting suspension was aged under ambient conditions for 24 h, which was then separated by centrifugation and washed with deionized water 3 times. After vacuum drying, the precipitate was calcined at 450 °C for 2 h to obtain the Au@ZnO nanospheres.

2.2. Characterization. The crystalline phases of the as-synthesized products were characterized by X-ray powder diffraction (XRD) using Rigaku D/max-2550 diffractometer (operated at 40 kV per 200 mA) with Cu Ka radiation (λ = 1.5406 Å). Data was collected over the 2θ range 20−80°. The morphologies and structures of the samples were recorded by field emission scanning electron microscopy (FESEM) using a JEOL JSM-7500F microscope, which was operated at 15 kV. Transmission electron microscopy (TEM), high resolution transmission electron microscopy (HRTEM) images, and the distribution of elements in crystal were conducted on a JEOL JEM-2100F microscopy operating at an accelerating voltage of 200 kV with an energy dispersive X-ray spectrometer.

3. RESULTS AND DISCUSSION

3.1. Structural and Morphological Characteristics. Figure 1 shows the typical XRD pattern of the as-prepared Au@ZnO yolk−shell nanospheres. As can be seen, the diffraction peaks indicated a mixed crystal phases of ZnO and Au, besides the peaks being indexed to wurtzite structured ZnO (JCPDS no. 36−1451) with lattice parameters a = 3.249 Å and c = 5.206 Å, the rest of the peaks were coincident with those from the standard card of cubic Au (JCPDS no. 4−784), no other crystalline phase corresponding to impurity was detected, which indicated that the product had a high purity.

As sacrificial templates, carbonaceous nanospheres play an important role in the fabrication of Au@ZnO yolk−shell nanostructure. The low-magnification FESEM image (Figure 2a) reveals that the as-synthesized template was composed of numerous spherical architectures with uniform size. The enlarged FESEM images in Figure 2b and c indicate that these homogeneous nanospheres had good monodispersity and the average diameter of nanospheres was about 500 nm. Furthermore, the panoramic TEM image in Figure 2d clearly

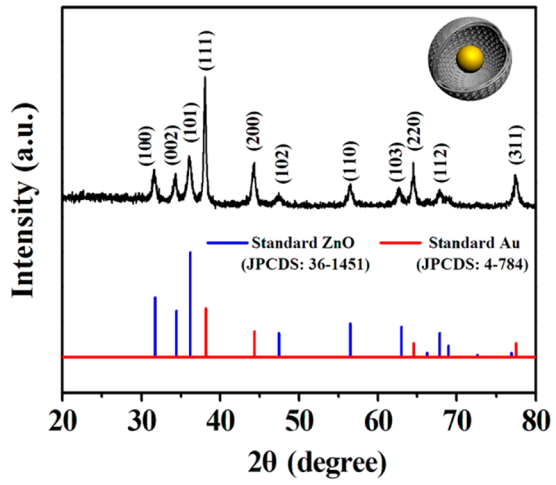

Figure 1. XRD pattern of the obtained Au@ZnO composites.

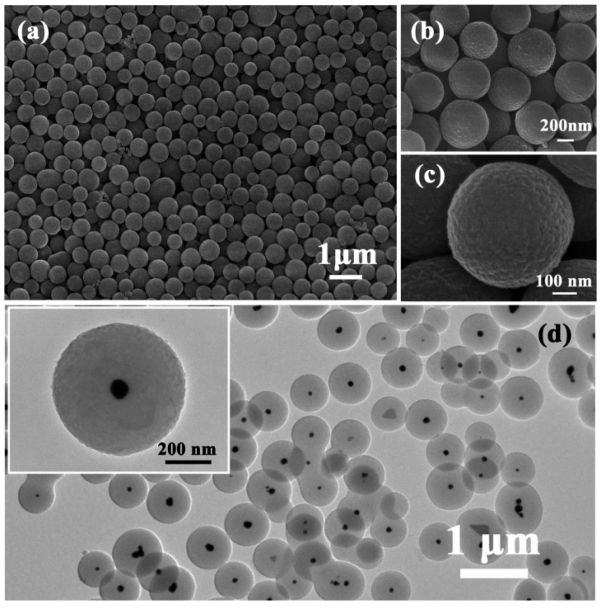

Figure 2. (a−c) SEM images of the Au@Carbon core−shell templates; (d) typical TEM images of Au@Carbon nanospheres after annealed at 450 °C for 2 h under an inert atmosphere.

shows the different contrast between the dark center and the light fringe, which confirmed that the Au nanoparticles had been encapsulated in the center of carbonaceous spheres successfully, forming a typical core−shell nanostructures. It can also be observed that the size of Au nanoparticles were about 50 nm (inset of Figure 2d).

After soaking in aqueous zinc acetate solution, the Au@carbon templates were calcined and eventually the Au@ZnO yolk−shell nanostructures were obtained. The microstructures and morphologies of the prepared Au@ZnO yolk−shell nanostructures were investigated by FESEM and TEM observations. As can be seen in Figure 3a, the as-synthesized Au@ZnO yolk−shell nanostructures were monodisperse and relatively uniform in size. The enlarged FESEM image (Figure 3b) shows that the Au@ZnO nanospheres had retained the original shapes of carbonaceous templates, but the diameter of Au@ZnO nanospheres was reduced to ∼55% (about 280 nm) in comparison with Au@carbon templates. In general, the surfaces of the carbonaceous templates are hydrophilic and

dx.doi.org/10.1021/am5057322 | ACS Appl. Mater. Interfaces 2014, 6, 18661−18667

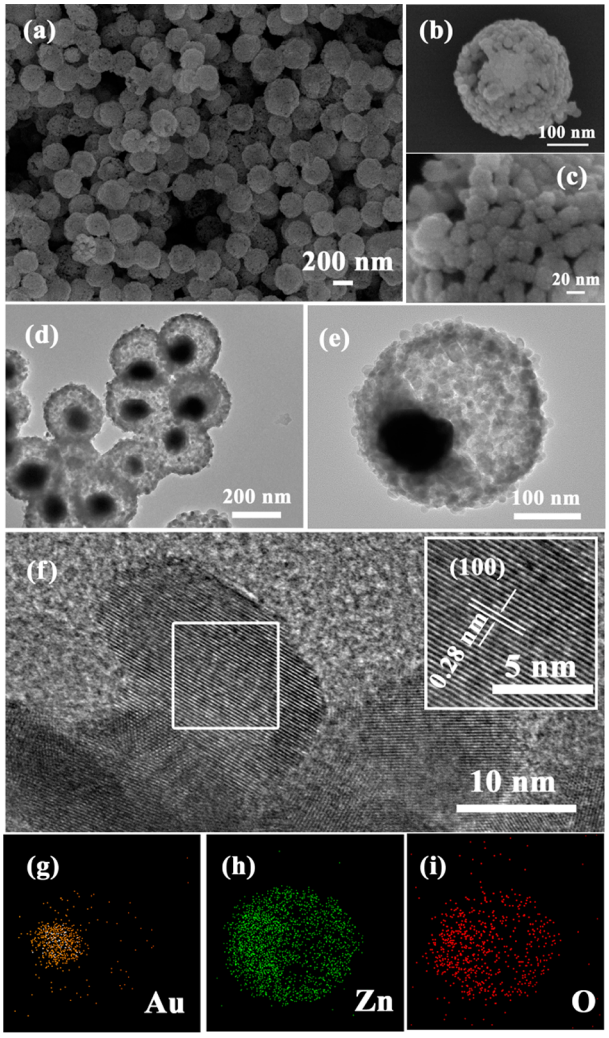

Figure 3. (a–c) FESEM images of Au@ZnO yolk–shell nanospheres with different magnifications; (d, e) typical TEM images of Au@ZnO composites; (f) HRTEM images; (g–i) elemental mapping of individual Au@ZnO nanosphere.

decorated with −OH and −C═O groups.[38] When these carbonaceous spheres were dispersed in aqueous zinc acetate solutions, the cations Zn^{2+} would bind with the functional groups on the surface layer. Accompany with the following calcination process, the carbonaceous templates shrinked gradually while the surface layers containing Zn^{2+} were condensed to accumulate sufficient mechanical strength to keep the well-defined configuration of ZnO hollow spheres, then the remarkable shrinkage would make sense.

The detailed morphology of the surface is shown in Figure 3c, it can be obviously seen that the Au@ZnO nanosphere had a rough and porous shell, which was built from many nanoparticles with a size of ∼20 nm. To further investigate the interior and the crystalline structure, the TEM and HRTEM observations were carried out. The low-magnification TEM image is presented in Figure 3d, from which the yolk–shell nanostructures got further confirmed. It should also be noted that most of the nanospheres were consisted of a single randomly distributed Au nanoparticle core and a porous ZnO shell, which indicated a high yield of these Au@ZnO yolk–shell nanostructures. The high-magnification TEM image shows the detailed morphological information on the nanostuctures. It can be observed that the shell thickness of nanospheres was about 40 nm. Moreover, nanometer-sized porous architectures were formed on surface, because of the densely stacking of ZnO nanoparticles, as shown in Figure 3e. The HRTEM image (Figure 3f) indicates that the nanoparticles on the shell of Au@ZnO nanostructure were single-crystalline. As can be seen from the inset of Figure 3f, the lattice spacing was about 0.28 nm, which corresponded to the distance between the {100}planes of the wurtzite ZnO. Figure 3g–i shows the TEM elemental mapping of the individual Au@ZnO nanosphere shown in Figure 3e. It is obvious that the signals of Au were mainly detected in the core region and barely in the shell region, whereas the signals of Zn and O distributed homogeneously within the 3D structure. These data also confirmed that the obtained nanosphere was built with two separate components.

3.2. Gas Sensing Properties. To prove such a unique structure might bring about more excellent gas sensing properties, two reference samples without the encapsulated Au nanoparticles were synthesized and characterized simultaneously (Details on the synthesis procedures and characterization results are supplied in Figure S1–S3 in the Supporting Information). Using the obtained ZnO solid nanospheres, ZnO hollow nanospheres, and Au@ZnO yolk–shell nanospheres as sensing materials, three gas sensors were fabricated and their gas sensing performances were investigated. The detailed fabrication procedure of sensor devices is as follows: the as-prepared samples were first mixed with deionized water to form a slurry, and then coated onto an alumina tube, at each end of which a pair of gold electrodes had been installed. In order to facilitate the signal collection, each gold electrode was connected with two platinum wires. Subsequently, a Ni–Cr alloy coil was placed through the alumina tube to control the operating temperature of the sensor. The structure of the sensor is schematically illustrated in Figure 4. Gas sensing

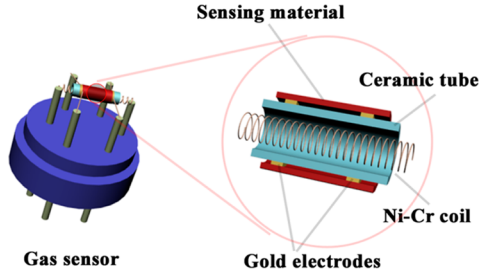

Figure 4. Structure schematic of a typical gas sensor.

measurements were processed by a static process under laboratory conditions (50 RH%, 25 °C). Here, the gas response was defined as the ratio of the resistance of the sensor in fresh air (R_a) to that in tested gases (R_g). The time taken by the sensor to achieve 90% of the total resistance change in the case of adsorbing and desorbing gas was defined as the response time (τ_{res}) and recovery time (τ_{recov}), respectively.

Figure 5 shows the response of three sensors to 100 ppm acetone at operating temperatures from 200 to 375 °C. From the pattern we can see that the responses of the tested sensors varied with operating temperature. It is well-known that the responses of sensors depend on the chemical reactions between the surface adsorbed oxygen species and the tested gas on the surface of oxides. At low temperatures the tested gas molecules do not have enough thermal energy to react with the surface adsorbed oxygen species. Therefore, the value of response is

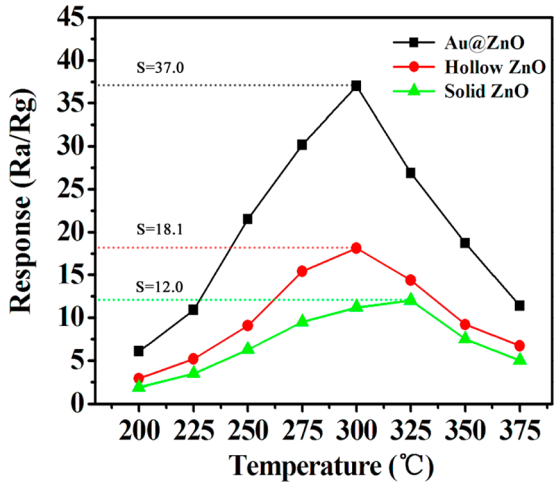

Figure 5. Responses of the sensor devices upon exposure to 100 ppm acetone at different working temperatures.

relatively low. With the increase of temperature, the gas molecules become activated enough to react with the surface adsorbed oxygen species, so a significant increase of response can be obtained. However, because of the diffculty in gas adsorption and the low utilization rate of sensing layer, the response of the sensor begins to decrease at higher temperature.[39,40] For ZnO solid nanospheres, the maximum response to 100 ppm acetone was 12, which obtained at 325 °C. For ZnO hollow nanospheres, the response first increased with the operating temperature, up to 300 °C, and then gradually decreased. The maximum response to acetone was 17.8. By contrast, the Au@ZnO composites, exhibited higher response at each temperature compared to the above two counterparts. Similarly, at the operating temperature of 300 °C, the sensor reached a maximum value of 37, which were almost two and three times higher than that of the obtained response of the ZnO hollow nanospheres and solid nanospheres.

The response characteristics of sensors toward different concentrations of acetone at optimal operating temperature are shown in Figure 6a. It is obvious that the corresponding responses of the sensors increased with the growth of acetone concentration from 10 to 700 ppm, and the sensor based on Au@ZnO yolk−shell nanostructure increased faster and displayed quite enhanced response. The responses of the three sensors depended near linearly on the gas concentrations in the full range, which indicated that the sensors have a broad detection range to acetone (inset of Figure 6a). Moreover, it is worth mentioning that the sensors using as-prepared ZnO nanospheres exhibit obvious response even for ppb-level acetone gas. As can be seen in Figure 6b, the gas responses to 200 ppb was about 2.3 and 1.4 for Au@ZnO yolk−shell nanospheres and ZnO hollow nanospheres. Therefore, the obtained gas sensors with low detection limit (200 ppb) might be used to monitor the trace amounts of acetone breathed out from a diabetic patient (the average concentration of acetone in the breath of a diabetic patient is believed to be higher than 1.8 ppm).[41,42] A comparison between the sensing performances of Au@ZnO nanospheres and some previously reported ZnO morphologies is summarized in Table 1. As can be seen, The sensor based on Au@ZnO yolk−shell nanostructure has a higher response and a lower detection limit than most other sensors, which confirmed that the Au@ZnO yolk−shell nanostructures maybe more suitable for gas sensing.

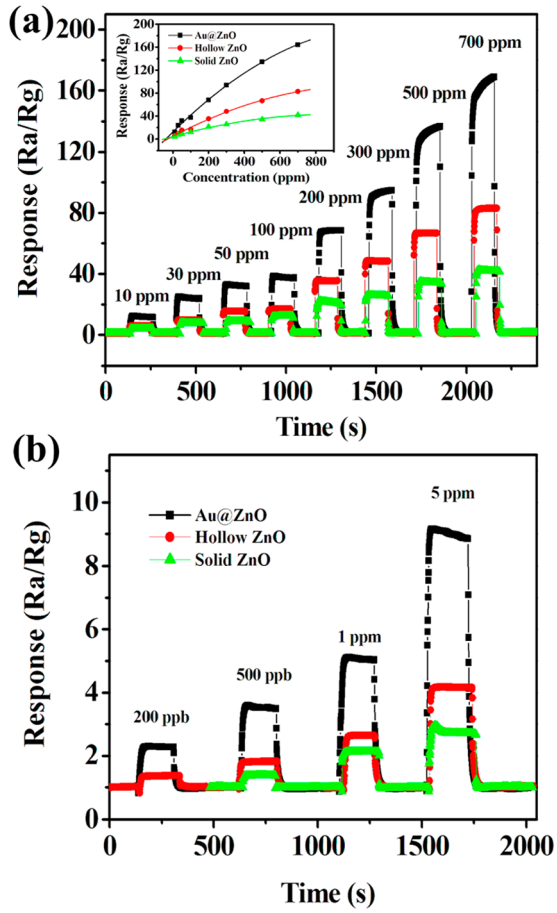

Figure 6. Responses of pure (solid and hollow) ZnO nanospheres and Au@ZnO composites versus acetone concentration in the range of (a) 10−700 ppm and (b) 200 ppb to 5 ppm at optimal operating temperature.

Table 1. Comparison of the Sensing Performances between the Current Work and Previous Results[43−46]

materials	operating temperature (°C)	acetone (ppm)	response	limit of detection (ppm)	ref
ZnO nanorods	300	100	30.4	1	43
dumbbell-like ZnO	300	100	26.1	~1	44
Co-doped ZnO nanofibers	360	100	~16	~5	45
Au-doped ZnO microspheres	325	200	2	≤100	46
Au@ZnO nanospheres	300	100	37	0.2	this work

Selectity is another important criterion of gas sensors. The response of the sensors based on ZnO hollow nanospheres and Au@ZnO composite to various volatile organic compounds (VOC) gases, such as formaldehyde, chloroform, acetone, methanol, xylene, and toluene is shown in Figure 7a. All of the gases were tested at an operating temperature of 300 °C with a concentration of 100 ppm. As expected, the sensor using the Au@ZnO yolk−shell nanospheres exhibited enhanced responses for each gas compared with that based on pure ZnO hollow nanospheres. It is also can be found that the Au@ZnO sensor displayed better response to acetone in comparison to

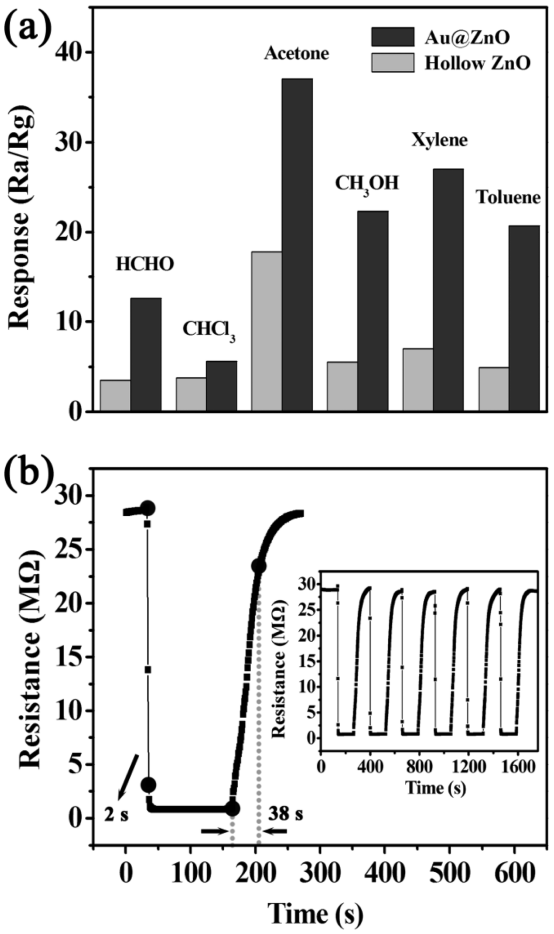

Figure 7. (a) Responses of sensors based on ZnO hollow nanospheres and Au@ZnO yolk–shell nanospheres to various gases (100 ppm); (b) dynamic response-recovery curves of Au@ZnO composites to 100 ppm acetone at 300 °C.

any other gases (Table S1 in the Supporting Information), indicating that the Au@ZnO nanospheres had good selectivity to acetone. And this good selectivity toward acetone also can be observed from the test results measured at low operating temperature as shown in Figure S4 in the Supporting Information. Moreover, Figure S5 in the Supporting Information presents the responses of Au@ZnO nanospheres toward various VOC gases at different operating temperature ranging from 200 to 350 °C. As can be seen, even when working at nonoptimal operating temperature, the sensor still showed higher response to acetone, but lower responses to other volatile organic compounds (VOC), which indicated that the sensor had a wide working temperature range.

The response and recovery characteristics, as an important criterion for evaluating the performance of gas sensors, are also investigated. Figure 7b displays the dynamic response-recovery curves of the Au@ZnO composite to 100 ppm acetone at 300 °C, and the results indicate that the sensor had a fast response-recovery process. The response time and recovery time were about 2 and 38 s, respectively. It can be also found that the sensor exhibited an excellent stability and reversibility when alternately exposed to air and acetone gas, as shown in the inset of Figure 7b. The sensing mechanism of metal oxides toward acetone can be described by modulation model of the depletion layer, which has been clarified in many previous works.[47,48] When the ZnO sensors were exposed to air, oxygen molecules in the air would adsorb on the surface of the ZnO and ionized to the chemisorbed oxygen species ($(O^{2-}$, O^- or $O_2^-)$ by extracting free electrons from the conduction band of ZnO. As a consequence, depletion layers were formed on the surface domains of ZnO, which led to an increase of resistance. If reducing gas such as acetone was introduced at this moment, acetone molecules would react with adsorbed oxygen species on the surface of ZnO. As a result, the trapped electrons were released back to the conduction band of ZnO, which eventually caused a remarkable decrease of resistance. The reaction involved above can be illustrated as follows

$$O_2 + e^- \leftrightarrow O_2^- \quad (1)$$

$$O_2^- + e^- \leftrightarrow 2O^- \quad (2)$$

$$O^- + e^- \leftrightarrow O^{2-} \quad (3)$$

$$CH_3COCH_3 + 8O^- \leftrightarrow 3CO_2 + 3H_2O + 8e^- \quad (4)$$

It is well-known that the working principle of gas sensor based on semiconductoroxides involves the receptor function, transducer function, and the utility factor of the sensing body.[49] Therefore, the concepts of sensor design are determined by considering these key factors. In this work, the distinctive configuration (hollow interiors and porous shells) endows ZnO hollow nanospheres and Au@ZnO composite plenty of pores, which can facilitate the diffusion of the test gas (utility factor) and improve the kinetics of the reaction between the test gas and surface adsorbed oxygen species (Figure 8a, b). For this reason, an improved sensitivity is observed in comparison with solid ZnO nanospheres. The ability of the sensing material to absorb and ionize oxygen species is fundamental to the performance of sensor. For Au@ZnO yolk–shell nanostructure, Au nanoparticle, as an active

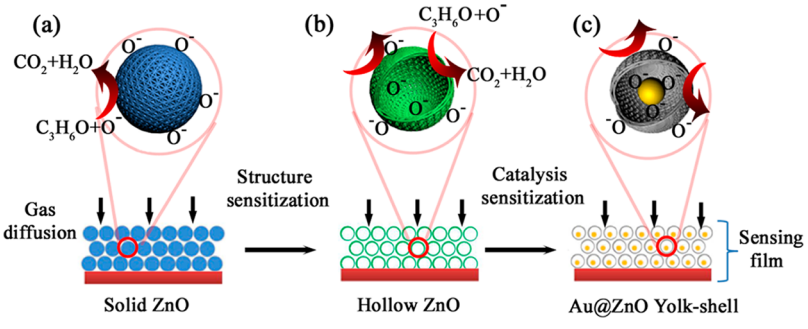

Figure 8. Gas sensing principles of (a) solid ZnO nanospheres, (b) hollow ZnO nanospheres, and (c) Au@ZnO nanospheres.

dx.doi.org/10.1021/am5057322 | ACS Appl. Mater. Interfaces 2014, 6, 18661–18667

component, can serve as an effective adsorption sites to bind and dissociate oxygen molecules (Figure 8c).[50,51] This process will increase the quantity of absorbed oxygen species, which results in a larger degree of electron extractions from the conduction band of ZnO. Therefore, the resistance of ZnO increased with the introduction of Au core as shown in Figure S6 in the Supporting Information. Because the response was defined as the ratio (R_a/R_g) between the resistances of the sensor in air (R_a) and in target gas (R_g), high baseline resistance will be conducive to increasing the response of gas sensor. Moreover, Au can break acetone into more active radicals and accelerate their reactions with absorbed oxygen species because of the well-known spillover effect of Au nanospheres.[52] Thus, the sensor based on yolk−shell Au@ZnO nanospheres showed better sensing performance than those based on hollow ZnO nanospheres. On the basis of the above discussion, we explain the observed dramatic enhancement of response in terms of the unique yolk−shell structure and the catalytic effect of Au nanoparticles.

4. CONCLUSIONS

In summary, uniform Au@ZnO yolk−shell nanostructures characterized by movable Au cores and porous ZnO shells have been successfully prepared by using Au@carbon nanospheres as hard templates. The obtained products were applied to sensor devices and their gas sensing properties were examined. It was found that the device based on as-prepared Au@ZnO composites exhibited an ultralow detection limit (200 ppb) and a higher response toward acetone in comparison to the pure ZnO nanostructures, which have confirmed the potential of Au@ZnO nanostructures for gas sensing applications. Moreover, the enhanced sensing performances have been demonstrated to be related to their unique microstructures and the catalytic effect of noble metal.

■ ASSOCIATED CONTENT

Supporting Information

Synthesis of ZnO hollow nanospheres, XRD pattern of ZnO hollow nanospheres, SEM images of carbonaceous nanospheres and ZnO hollow nanospheres, synthesis of ZnO solid nanospheres, XRD pattern and SEM images of as-obtained solid ZnO nanospheres, response of the sensor to various test gases at 300 °C, response of the sensors to various test gases at 200 °C, responses of the sensor based on Au@ZnO nanospheres to 100 ppm various tested gases as a function of operating temperature, and dynamic response-recovery curves of the sensor based on Au@ZnO composite and pure hollow ZnO to 100 ppm acetone at 300 °C. This material is available free of charge via the Internet at http://pubs.acs.org/.

■ AUTHOR INFORMATION

Corresponding Authors

*E-mail: spmaster2008@163.com. Fax: +86 431 85167808. Tel: +86 431 8516780.

*E-mail: lugy@jlu.edu.cn.

Notes

The authors declare no competing financial interest.

■ ACKNOWLEDGMENTS

This work is supported by the National Nature Science Foundation of China (61074172, 61134010, and 61327804), the Program for Chang Jiang Scholars and Innovative Research Team in University (IRT13018), and the National High-Tech Research and Development Program of China (863 Program, 2013AA030902).

■ ABBREVIATIONS

XRD, X-ray powder diffraction
FESEM, field-emission scanning electron microscopy
TEM, transmission electron microscopy
HRTEM, high-resolution transmission electron microscopy
VOC, volatile organic compounds

■ REFERENCES

(1) Liu, X.; Cheng, S.; Liu, H.; Hu, S.; Zhang, D.; Ning, H. A Survey on Gas Sensing Technology. *Sensors* **2012**, *12*, 9635−9665.
(2) Alenezi, M. R.; Henley, S. J.; Emerson, N. G.; Silva, S. R. P. From 1D and 2D ZnO Nanostructures to 3D Hierarchical Structures with Enhanced Gas Sensing Properties. *Nanoscale* **2013**, *6*, 235−247.
(3) Kruefu, V.; Liewhiran, C.; Wisitsoraat, A.; Phanichphant, S. Selectivity of Flame-Spray-Made Nb/ZnO Thick Films Towards NO_2 Gas. *Sens. Actuators, B* **2011**, *156*, 360−367.
(4) Sun, P.; Liu, Y.; Li, X.; Sun, Y.; Liang, X.; Liu, F.; Lu, G. Facile Synthesis and Gas-Sensing Properties of Monodisperse α-Fe_2O_3 Discoid Crystals. *RSC Adv.* **2012**, *2*, 9824−9829.
(5) Fine, G. F.; Cavanagh, L. M.; Afonja, A.; Binions, R. Metal Oxide Semi-Conductor Gas Sensors in Environmental Monitoring. *Sensors* **2010**, *10*, 5469−5502.
(6) Sun, Y. F.; Liu, S. B.; Meng, F. L.; Liu, J. Y.; Jin, Z.; Kong, L. T.; Liu, J. H. Metal Oxide Nanostructures and Their Gas Sensing Properties: A Review. *Sensors* **2012**, *12*, 2610−2631.
(7) Wahab, R.; Ansari, S. G.; Kim, Y. S.; Seo, H. K.; Kim, G. S.; Khang, G.; Shin, H.-S. Low Temperature Solution Synthesis and Characterization of ZnO Nano-Flowers. *Mater. Res. Bull.* **2007**, *42*, 1640−1648.
(8) Zhang, H.; Wu, R.; Chen, Z.; Liu, G.; Zhang, Z.; Jiao, Z. Self-Assembly Fabrication of 3D Flower-Like ZnO Hierarchical Nanostructures and Their Gas Sensing Properties. *CrystEngComm* **2012**, *14*, 1775−1782.
(9) Sun, P.; You, L.; Wang, D. W.; Sun, Y. F.; Ma, J.; Lu, G. Y. Synthesis and Gas Sensing Properties of Bundle-Like Alpha-Fe_2O_3 Nanorods. *Sens. Actuators, B* **2011**, *156*, 368−374.
(10) Volanti, D. P.; Orlandi, M. O.; Andres, J.; Longo, E. Efficient Microwave-Assisted Hydrothermal Synthesis of CuO Sea Urchin-Like Architectures via A Mesoscale Self-Assembly. *CrystEngComm* **2010**, *12*, 1696−1699.
(11) Zhao, H.; Dong, H. X.; Zhang, L. N.; Wang, X. W.; Yang, H. Q. Controlled Synthesis and Photocatalytic Properties of Porous Hollow In_2O_3 Microcubes with Different Sizes. *Mater. Chem. Phys.* **2011**, *130*, 921−931.
(12) Tseng, W. J.; Tseng, T.-T.; Wu, H.-M.; Her, Y.-C.; Yang, T.-J.; Gouma, P. Facile Synthesis of Monodispersed In_2O_3 Hollow Spheres and Application in Photocatalysis and Gas Sensing. *J. Am. Ceram. Soc.* **2013**, *96*, 719−725.
(13) Li, X. W.; Sun, P.; Yang, T. L.; Zhao, J.; Wang, Z. Y.; Wang, W. N.; Liu, Y. P.; Lu, G. Y.; Du, Y. Template-Free Microwave-Assisted Synthesis of ZnO Hollow Microspheres and Their Application in Gas Sensing. *CrystEngComm* **2013**, *15*, 2949−2955.
(14) Singh, N.; Ponzoni, A.; Gupta, R. K.; Lee, P. S.; Comini, E. Synthesis of In_2O_3-ZnO Core-Shell Nanowires and Their Application in Gas Sensing. *Sens. Actuators, B* **2011**, *160*, 1346−1351.
(15) Zhong, J.; Cao, C.; Liu, Y.; Li, Y.; Khan, W. S. Hollow Core−Shell η-Fe_2O_3 Microspheres with Excellent Lithium-Storage and Gas-Sensing Properties. *Chem. Commun.* **2010**, *46*, 3869−3871.
(16) Wu, H. B.; Pan, A.; Hng, H. H.; Lou, X. W. D. Template-Assisted Formation of Rattle-type V_2O_5 Hollow Microspheres with Enhanced Lithium Storage Properties. *Adv. Funct. Mater.* **2013**, *23*, 5669−5674.
(17) Liu, J.; Qiao, S. Z.; Budi Hartono, S.; Lu, G. Q. Monodisperse Yolk-Shell Nanoparticles with a Hierarchical Porous Structure for

Delivery Vehicles and Nanoreactors. *Angew. Chem., Int. Ed.* **2010**, *49*, 4981−4985.
(18) Fang, W. Q.; Yang, X. H.; Zhu, H.; Li, Z.; Zhao, H.; Yao, X.; Yang, H. G. Yolk@Shell Anatase TiO_2 Hierarchical Microspheres with Exposed {001} Facets for High-Performance Dye Sensitized Solar Cells. *J. Mater. Chem.* **2012**, *22*, 22082−22089.
(19) Choi, E.; Kwak, M.; Jang, B.; Piao, Y. Highly Monodisperse Rattle-Structured Nanomaterials with Gold Nanorod Core-Mesoporous Silica Shell as Drug Delivery Vehicles and Nanoreactors. *Nanoscale* **2013**, *5*, 151−154.
(20) Hong, Y. J.; Son, M. Y.; Kang, Y. C. One-Pot Facile Synthesis of Double-Shelled SnO_2 Yolk-Shell-Structured Powders by Continuous Process as Anode Materials for Li-Ion Batteries. *Adv. Mater.* **2013**, *25*, 2279−2283.
(21) Lu, G. Y.; Xu, J.; Sun, J. B.; Yu, Y. S.; Zhang, Y. Q.; Liu, F. M. UV-Enhanced Room Temperature NO_2 Sensor Using ZnO Nanorods Modified with SnO_2 Nanoparticles. *Sens. Actuators, B* **2012**, *162*, 82−88.
(22) Lin, C. H.; Liu, X. y.; Wu, S. H.; Liu, K. H.; Mou, C. Y. Corking and Uncorking a Catalytic Yolk-Shell Nanoreactor: Stable Gold Catalyst in Hollow Silica Nanosphere. *J. Phys. Chem. Lett.* **2011**, *2*, 2984−2988.
(23) Su, W.; Zhang, T.; Li, L.; Xing, J.; He, M.; Zhong, Y.; Li, Z. Synthesis of Small Yolk−Shell Fe_3O_4@TiO_2 Nanoparticles with Controllable Thickness as Recyclable Photocatalysts. *RSC Adv.* **2014**, *4*, 8901−8906.
(24) Güttel, R.; Paul, M.; Schüth, F. Activity Improvement of Gold Yolk−Shell Catalysts for CO Oxidation by Doping with TiO_2. *Catal. Sci. Technol.* **2011**, *1*, 65−68.
(25) Lee, J.; Park, J. C.; Song, H. A Nanoreactor Framework of a Au@SiO_2 Yolk/Shell Structure for Catalytic Reduction of p-Nitrophenol. *Adv. Mater.* **2008**, *20*, 1523−1528.
(26) Lee, J.; Park, J. C.; Bang, J. U.; Song, H. Precise Tuning of Porosity and Surface Functionality in Au@SiO_2 Nanoreactors for High Catalytic Efficiency. *Chem. Mater.* **2008**, *20*, 5839−5844.
(27) Guo, H.; Wang, W.; Liu, L.; He, Y.; Li, C.; Wang, Y. Shape-Controlled Synthesis of Ag@TiO_2 Cage-Bell Hybrid Structure with Enhanced Photocatalytic Activity and Superior Lithium Storage. *Green Chem.* **2013**, *15*, 2810−2816.
(28) Lee, I.; Joo, J. B.; Yin, Y.; Zaera, F. A Yolk@Shell Nanoarchitecture for Au/TiO_2 Catalysts. *Angew. Chem.* **2011**, *123*, 10390−10393.
(29) Wang, L. L.; Dou, H. M.; Lou, Z.; Zhang, T. Encapsuled Nanoreactors (Au@SnO_2): A New Sensing Material for Chemical Sensors. *Nanoscale* **2013**, *5*, 2686−2691.
(30) Liu, J.; Qiao, S. Z.; Chen, J. S.; Lou, X. W.; Xing, X.; Lu, G. Q. Yolk/Shell Nanoparticles: New Platforms for Nanoreactors, Drug Delivery and Lithium-ion Batteries. *Chem. Commun.* **2011**, *47*, 12578−12591.
(31) Du, J.; Qi, J.; Wang, D.; Tang, Z. Facile Synthesis of Au@TiO_2 Core−Shell Hollow Spheres for Dye-Sensitized Solar Cells with Remarkably Improved Efficiency. *Energy Environ. Sci.* **2012**, *5*, 6914−6918.
(32) Wei, Z.; Zhou, Z.; Yang, M.; Lin, C.; Zhao, Z.; Huang, D.; Chen, Z.; Gao, J. Multifunctional Ag@Fe_2O_3 Yolk−Shell Nanoparticles for Simultaneous Capture, Kill, and Removal of Pathogen. *J. Mater. Chem.* **2011**, *21*, 16344−16348.
(33) Kim, M.; Park, J. C.; Kim, A.; Park, K. H.; Song, H. Porosity Control of Pd@SiO_2 Yolk-Shell Nanocatalysts by The Formation of Nickel Phyllosilicate and Its Influence on Suzuki Coupling Reactions. *Langmuir* **2012**, *28*, 6441−6447.
(34) Zhang, N.; Fu, X.; Xu, Y.-J. A Facile and Green Approach to Synthesize Pt@CeO_2 Nanocomposite with Tunable Core-Shell and Yolk-Shell Structure and Its Application as A Visible Light Photocatalyst. *J. Mater. Chem.* **2011**, *21*, 8152−8158.
(35) Liu, X.; Zhang, J.; Wang, L.; Yang, T.; Guo, X.; Wu, S.; Wang, S. 3D Hierarchically Porous ZnO Structures and Their Functionalization by Au Nanoparticles for Gas Sensors. *J. Mater. Chem.* **2011**, *21*, 349−356.
(36) Wang, L. L.; Lou, Z.; Fei, T.; Zhang, T. Templating Synthesis of ZnO Hollow Nanospheres Loaded with Au Nanoparticles and Their Enhanced Gas Sensing Properties. *J. Mater. Chem.* **2012**, *22*, 4767−4771.
(37) Wang, J.; Zou, B.; Ruan, S.; Zhao, J.; Wu, F. Synthesis, Characterization, and Gas-Sensing Property for HCHO of Ag-Doped In_2O_3 Nanocrystalline Powders. *Mater. Chem. Phys.* **2009**, *117*, 489−493.
(38) Sun, X.; Liu, J.; Li, Y. Use of Carbonaceous Polysaccharide Microspheres as Templates for Fabricating Metal Oxide Hollow Spheres. *Chem.—Eur. J.* **2006**, *12*, 2039−2047.
(39) Neri, G.; Bonavita, A.; Micali, G.; Rizzo, G.; Callone, E.; Carturan, G. Resistive CO Gas Sensors Based on In_2O_3 and $InSnO_x$ Nanopowders Synthesized via Starch-Aided Sol−Gel Process for Automotive Applications. *Sens. Actuators, B* **2008**, *132*, 224−233.
(40) Sun, P.; Zhou, X.; Wang, C.; Shimanoe, K.; Lu, G.; Yamazoe, N. Hollow SnO_2/α-Fe_2O_3 Spheres with Double-Shell Structure for Gas Sensor. *J. Mater. Chem. A* **2013**, *2*, 1302−1308.
(41) Deng, C.; Zhang, J.; Yu, X.; Zhang, W.; Zhang, X. Determination of Acetone in Human Breath by Gas Chromatography−Mass Spectrometry and Solid-Phase Microextraction with On-Fiber Derivatization. *J. Chromatogr. B* **2004**, *810*, 269−275.
(42) Wang, L.; Teleki, A.; Pratsinis, S. E.; Gouma, P. I. Ferroelectric WO_3 Nanoparticles for Acetone Selective Detection. *Chem. Mater.* **2008**, *20*, 4794−4796.
(43) Zeng, Y.; Zhang, T.; Yuan, M. X.; Kang, M. H.; Lu, G. Y.; Wang, R.; Fan, H. T.; He, Y.; Yang, H. B. Growth and Selective Acetone Detection Based on ZnO Nanorod Arrays. *Sens. Actuators, B* **2009**, *143*, 93−98.
(44) Qi, Q.; Zhang, T.; Liu, L.; Zheng, X. J.; Yu, Q. J.; Zeng, Y.; Yang, H. B. Selective Acetone Sensor Based on Dumbbell-Like ZnO with Rapid Response and Recovery. *Sens. Actuators, B* **2008**, *134*, 166−170.
(45) Liu, L.; Li, S.; Zhuang, J.; Wang, L.; Zhang, J.; Li, H.; Liu, Z.; Han, Y.; Jiang, X.; Zhang, P. Improved Selective Acetone Sensing Properties of Co-Doped ZnO Nanofibers by Electrospinning. *Sens. Actuators, B* **2011**, *155*, 782−788.
(46) Li, X.; Feng, W.; Xiao, Y.; Sun, P.; Hu, X.; Shimanoe, K.; Lu, G.; Yamazoe, N. Hollow Zinc Oxide Microspheres Functionalized by Au Nanoparticles for Gas Sensors. *RSC Adv.* **2014**, *4*, 28005−28010.
(47) Wei, S.; Zhou, M.; Du, W. Improved Acetone Sensing Properties of ZnO Hollow Nanofibers by Single Capillary Electrospinning. *Sens. Actuators, B* **2011**, *160*, 753−759.
(48) Xiao, Y.; Lu, L.; Zhang, A.; Zhang, Y.; Sun, L.; Huo, L.; Li, F. Highly Enhanced Acetone Sensing Performances of Porous and Single Crystalline ZnO Nanosheets: High Percentage of Exposed (100) Facets Working Together with Surface Modification with Pd Nanoparticles. *ACS Appl. Mater. Interfaces* **2012**, *4*, 3797−3804.
(49) Yamazoe, N.; Shimanoe, K. New Perspectives of Gas Sensor Technology. *Sens. Actuators, B* **2009**, *138*, 100−107.
(50) Min, B. K.; Friend, C. M. Heterogeneous Gold-Based Catalysis for Green Chemistry: Low-Temperature CO Oxidation and Propene Oxidation. *Chem. Rev.* **2007**, *107*, 2709−2724.
(51) Janssens, T. V. W.; Carlsson, A.; Puig-Molina, A.; Clausen, B. S. Relation Between Nanoscale Au Particle Structure and Activity for CO Oxidation on Supported Gold Catalysts. *J. Catal.* **2006**, *240*, 108−113.
(52) Yamazoe, N.; Kurokawa, Y.; Seiyama, T. Effects of Additives on Semiconductor Gas Sensors. *Sens. Actuators* **1983**, *4*, 283−289.